ACADEMIC PRESS

Available online at www.sciencedirect.com
SCIENCE DIRECT®

Journal of Catalysis 217 (2003) 343–353

JOURNAL OF CATALYSIS

www.elsevier.com/locate/jcat

Nanometric monodispersed titanium oxide particles on mesoporous silica: synthesis, characterization, and catalytic activity in oxidation reactions in the liquid phase

A. Tuel * and L.G. Hubert-Pfalzgraf

Institut de Recherches sur la Catalyse, CNRS 2, avenue Albert Einstein, 69626 Villeurbanne Cedex, France

Received 17 October 2002; revised 7 February 2003; accepted 12 February 2003

Abstract

Subnanometric monodispersed titanium oxide particles have been dispersed on the surface of a large mesopore SBA-15 silica. TiSBA-15 materials were obtained by reaction between a hexanuclear titanium oxo cluster and a calcined SBA-15 silica in solution. Solids with various Ti loading have been prepared and characterized by chemical analysis, X-ray diffraction, nitrogen adsorption, and UV–visible spectroscopy. Titanium oxide particles containing 6 Ti octahedra show a UV–visible absorption band at ca. 235 nm, close to those usually observed on TiMCM-41 or TiHMS materials obtained by direct synthesis. The catalytic performance of TiSBA compounds has been evaluated in a series of oxidation reactions with H_2O_2 or TBHP as oxygen donors and compared with that of TiHMS materials obtained by direct synthesis. Data indicate that TiO_2 nanoparticles are active and selective in epoxidation of cyclohexene and in oxidation of aniline and aromatic molecules. Activities and selectivities suggest that isolated tetrahedrally coordinated Ti species are not necessarily the only active species for these reactions. Moreover, results raise the problem of the validity of such oxidation reactions as a test for the determination of the coordination state of Ti species.
© 2003 Elsevier Science (USA). All rights reserved.

Keywords: Hexanuclear titanium cluster; Mesoporous silica; SBA-15; Selective oxidation; Hydrogen peroxide

1. Introduction

The couple SiO_2–TiO_2 has been known for a long time as an efficient catalyst in oxidation reactions in the liquid phase using hydrogen peroxide or alkylhydroperoxides as oxygen donors. Preliminary catalysts, obtained by dispersing a titanium precursor on the surface of silica, showed interesting activities and selectivities in the epoxidation of 1-octene with *tert*-butyl hydroperoxide (TBHP) [1–3]. About 10 years later, Taramasso et al. reported the synthesis of TS-1, a titanium-substituted silicalite-1 [4]. This zeolite was particularly active and selective in the oxidation and hydroxylation of small substrates with dilute H_2O_2 solutions [5,6]. These properties promoted the development of new catalytic systems, based on zeolitic or amorphous materials. In particular, the recent discovery of Ti-substituted mesoporous molecular sieves opened new opportunities in selective oxidation of bulky substrates [7–15].

In zeolites, the activity has been attributed to isolated, generally tetrahedrally coordinated, framework Ti species [16–19]. Indeed, when TS-1 is prepared in the presence of an excess of titanium, extraframework oxide particles are formed and the activity strongly decreases. The situation is more complicated in mesoporous silicas. Zhang et al. have reported that TiMCM-41 or TiHMS materials actually contain Ti species with 4-, 5-, and 6-fold coordination [20]. Although the higher coordination sites most likely result from hydration of tetrahedrally coordinated Ti species, the presence of TiO_2 nanoparticles inside the mesopores cannot be excluded, especially in Ti-rich materials. The influence of such particles on the catalytic properties of the corresponding solids is quite difficult to estimate due to the simultaneous presence of Ti species with different coordination states. Whereas some publications report that the activity of Ti-containing mesoporous silicas has a tendency to decrease with the Ti loading, with a maximum around 1–2 wt% Ti [21], other data show very high performances for compounds containing up to 10 wt% Ti [12,22]. The reason is that many factors like the preparation route, the activation,

* Corresponding author.
E-mail address: tuel@catalyse.univ-lyon1.fr (A. Tuel).

0021-9517/03/$ – see front matter © 2003 Elsevier Science (USA). All rights reserved.
doi:10.1016/S0021-9517(03)00078-2

and the hydrophilic character of the surface also greatly influence the catalytic behavior. Moreover, the TiO_2 particle size and the particle-size distribution probably also modify the activity and selectivity. Unfortunately, these parameters are rarely reported since they are difficult to control at constant Ti loading, especially in the case of very small particles. In most cases, the presence of polycondensed Ti species is qualitatively estimated from the presence of signals above 250 nm in the UV–visible spectrum of the catalyst.

In the present work, subnanometric monodispersed TiO_2 particles containing 6 Ti atoms have been supported on a mesoporous SBA-15 silica. This was achieved by grafting a hexanuclear titanium oxo carboxylato alkoxide cluster $[Ti_6(\mu_3\text{-}O)_6(\mu\text{-}O_2CC_6H_4OPh)_6(OEt)_6]$, further denoted as "$Ti_6$ cluster," on the surface of a calcined SBA-15 silica. The obtained materials were characterized by chemical analysis, X-ray diffraction, nitrogen adsorption, and UV–visible spectroscopy and used as catalysts in a series of oxidation reactions using either H_2O_2 or TBHP as oxidizing agent. Their performances were compared with those of standard Ti-containing mesoporous silicas prepared by direct synthesis and having similar Ti loading.

2. Experimental

2.1. Synthesis of Ti_6 cluster

The hexanuclear cluster $[Ti_6(\mu_3\text{-}O)_6(\mu\text{-}O_2CC_6H_4OPh)_6(OEt)_6]$ (Fig. 1) was prepared according to a published procedure [23]. The purity of the compound was established using FT-IR spectroscopy. After drying, 440 mg of the cluster was dissolved in 25 mL of tetrahydrofuran (THF) and the Ti_6 solution thus obtained was kept under inert atmosphere.

2.2. Synthesis of SBA-15

The synthesis of the mesoporous molecular sieve SBA-15 was adapted from a recipe reported by Zhao et al. [24]. Tetraethylorthosilicate (TEOS) and poly(ethylene oxide)-*block*-poly(propylene oxide)-*block*-poly(ethylene oxide) triblock copolymer (Aldrich, $M_{avg} = 5800$, $EO_{20}PO_{70}EO_{20}$, P123) were used as silica source and structure-directing agent, respectively. The mesoporous silica was then calcined in air at 500 °C for 12 h to remove organics. Pure silica SBA-15 was characterized by X-ray diffraction and nitrogen adsorption.

2.3. Grafting procedure

Three catalysts with Ti loading corresponding to $Si/Ti = 30$, 50, and 100 have been prepared. In a typical preparation, the required amount of Ti_6 solution was added to 100 mL of THF under argon. One gram of calcined SBA-15, preliminary dehydrated in an oven at 150 °C for 24 h, was then added and the mixture was refluxed for 20 h under stirring. The solid was then recovered by filtration, washed with dry THF, and air-dried at room temperature. Part of the solid was further calcined in air at 550 °C for 15 h.

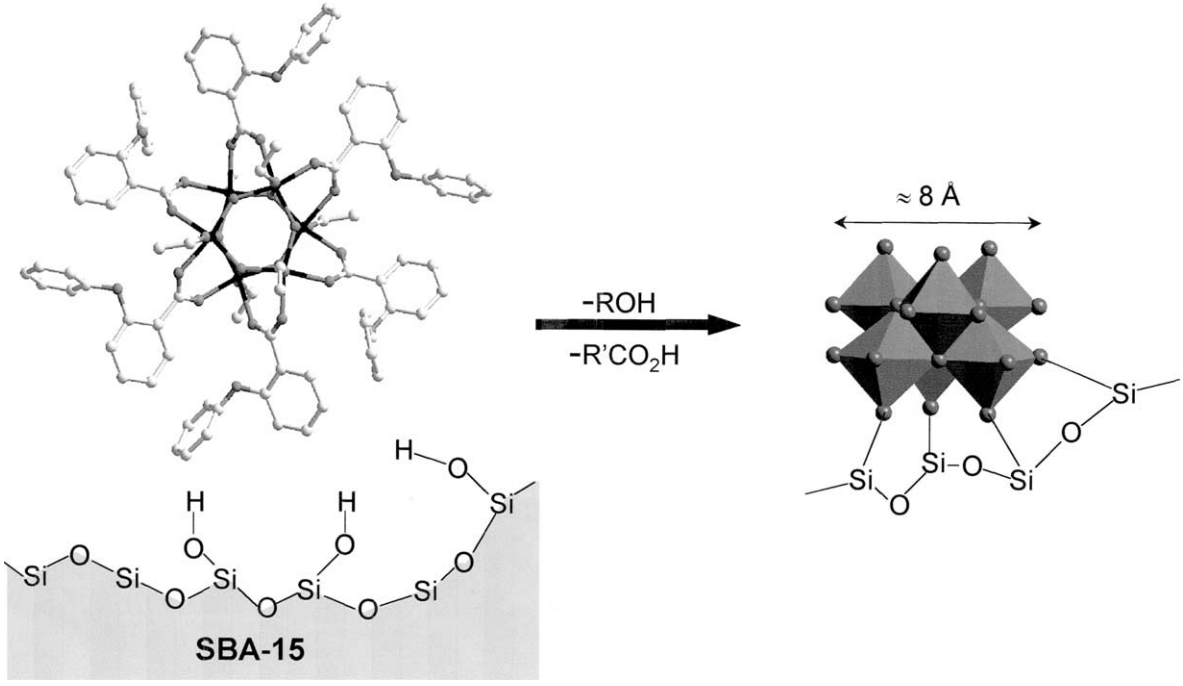

Fig. 1. Ball-and-stick representation of the $[Ti_6(\mu_3\text{-}O)_6(\mu\text{-}O_2CC_6H_4OPh)_6(OEt)_6]$ cluster (white, C; gray, O; and black, Ti atoms) and assembly of TiO_6 tetrahedra after elimination of organics and grafting on SBA-15.

2.4. Synthesis of Ti-HMS molecular sieves

TiHMS molecular sieves were prepared using hexadecylamine as surfactant following a recipe of the literature [25]. Four samples with Si/Ti ratios of 10, 30, 50, and 100 were prepared. Amine molecules were removed in boiling ethanol and extracted materials were further calcined in air at 500 °C to remove traces of organics.

2.5. Characterization techniques

Catalysts were characterized by X-ray diffraction, nitrogen adsorption, and UV–visible spectroscopy. The Ti content was determined by atomic adsorption after dissolution of the samples in HF:HCl solutions.

X-ray diffraction patterns were recorded between 1° and 10° (2θ) on a Bruker (Siemens) D5005 diffractometer using Cu-K_{α_2} radiation with steps of 0.02° and 10 s per step.

N_2 adsorption/desorption isotherms were collected at 77 K using a Catasorb analyzer. Samples were preliminary evacuated under vacuum at 500 °C overnight.

UV–visible spectra were obtained on a Varian Lambda 9 spectrometer in the region between 200 and 1000 cm^{-1}.

Thermal analysis data were collected on a SETERAM TGDSC 111 apparatus connected to a mass spectrometer. As-made TiSBA compounds were heated in air from 25 to 750 °C at a heating rate of 5 °C/min.

2.6. Catalytic reactions

Catalysts have been tested in the following reactions: epoxidation of cyclohexene, oxidation of aniline, oxidation of 2,6-di-*tert*-butylphenol (DTBP) and oxidation of 2,3,6-trimethylphenol (TMP). All reactions were performed under ambient atmosphere in a round-bottom flask equipped with a condenser and a magnetic stirrer. The catalyst was dispersed in a solvent containing the substrate and the temperature was increased. After stabilization of the temperature, the oxidizing agent (H_2O_2, 30 wt% in water or TBHP, 95 wt% in cyclohexane) was added dropwise. Samples were taken at regular time intervals and analyzed by gas chromatography using a Carbowax (AT-Wax) column (Alltech) attached to a FID. The H_2O_2 or TBHP conversions were determined by iodometric titration. Additional experimental details like the reaction temperature, the nature of the solvent, or the amount of catalyst are reported for each reaction in the corresponding section.

3. Results and discussion

3.1. Synthesis

The structurally well-defined $Ti_6(\mu_3\text{-}O)_6(OEt)_6(\mu\text{-}O_2CC_6H_4OPh)_6$ carboxylato alkoxide was selected as the source of TiO_2 particles. The presence of triply bridging oxo ligands, of 6-coordinated metals, of ancillary ligands displaying differential hydrolysis [26–28], is a favorable feature for controlled hydrolysis and/or grafting via Si–OH bonds. The metallic part of the cluster can be assimilated to a round-shaped particle with a diameter of ca. 8 Å (Fig. 1). It consists of two staggered triangular units built by sharing vertices of TiO_6 octahedra, which are joined by six common edges. The Ti_6 cluster was dissolved under inert atmosphere in anhydrous THF. The high dilution of the medium as well as the homogeneity of the solution account for the absence of extensive condensation in solution prior to grafting. Immobilization of the cluster on the surface involves the most labile linkages namely the Ti–OEt ones in the first step and proceeds by elimination of alcohol (Fig. 1). Heating promotes elimination of the remaining organic ligands either by intramolecular elimination of ester or by hydrolysis of the $M\text{–}O_2CR'$ bonds. TGA data indicate that nearly all organics have been eliminated at the end of the refluxing. Hydrolytic or nonhydrolytic condensation of the clusters on the surface, although not impossible, is not very likely in view of the dilution used.

3.2. Characterization of SBA-15 and modified SBA-15 materials

SBA-15 possesses a highly ordered large mesopores hexagonal structure with mesopore diameters usually of between 60 and 100 Å [29,30]. This material is thus an excellent candidate for supporting large complexes like the Ti_6 cluster, which cannot easily penetrate the relatively small mesopores of standard MCM-41 silica. The XRD pattern of the calcined SBA-15 silica shows five reflections, characteristic of a highly ordered hexagonal structure, that can be indexed to (100), (110), (200), (210), and (300) with a unit cell parameter $a_0 = 106$ Å (Fig. 2). This observation is in agreement with that of previous reports on the same type of materials. The nitrogen adsorption/desorption isotherm is shown in Fig. 3. The isotherm (type IV) with H_1-type hysteresis is typical of mesoporous materials with one-dimensional cylindrical channels. Calcined SBA-15 has a BET surface area of 987 ± 7 m^2/g and a pore volume of 1.35 mL/g (Table 1). The pore-size distribution, calculated on the desorption branch of the isotherm, is narrow and centered around 66 Å. From the latter value, the wall thickness can be estimated to ca. 40 Å. Assuming that the totality of the surface is accessible to Ti_6 clusters, it is possible to calculate the Si/Ti ratio corresponding to a complete coverage. The hexanuclear cluster can be assimilated to a disk with a diameter of ca. 1.8 nm, and this leads to a Si/Ti ratio of 5 for a monolayer. However, it was recently reported that the silica walls of SBA-15 are not uniform, the large mesopores being surrounded by a microporous corona [31]. These micropores are not accessible to large molecules like Ti_6 clusters. Even though the fraction of micropores is difficult to estimate, it is clear that nitrogen adsorption overestimates the surface effectively accessible to the clusters. The Si/Ti ratio in the

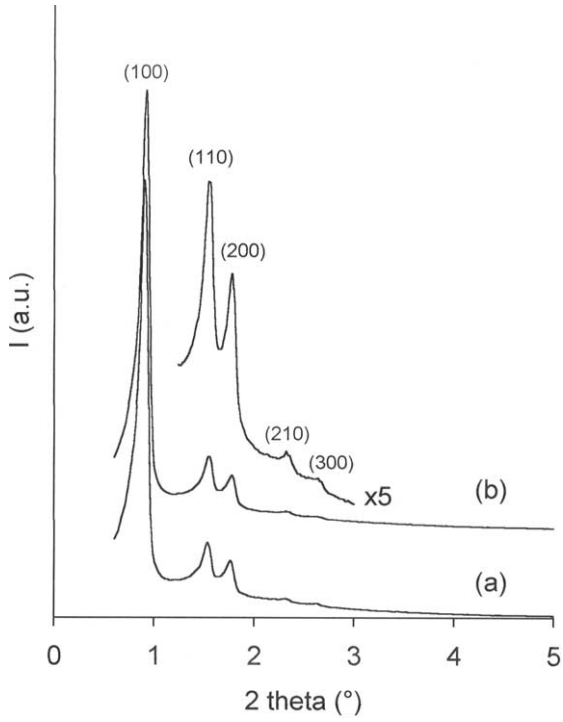

Fig. 2. X-ray diffraction patterns of calcined SBA-15 (a) and TiSBA-30 (b).

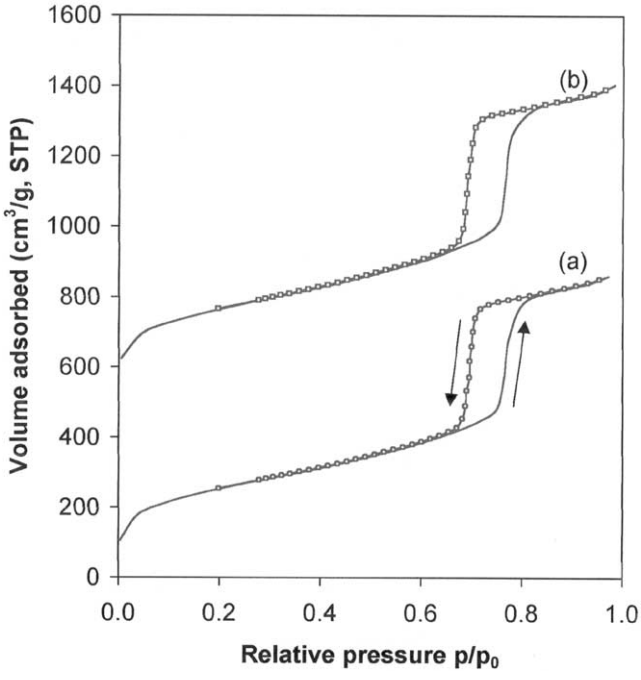

Fig. 3. Nitrogen adsorption/desorption isotherms on SBA-15 (a) and TiSBA-30 (b) materials.

grafted samples was thus varied between 30 and 100. This range ensures a high dilution of the Ti precursor in THF and, thus, a good dispersion of the clusters on silica.

Chemical analysis shows that the Si/Ti ratios in the grafted materials are almost the same as those of the precursor solutions (Table 1). This indicates that the totality of the molecules have been grafted on the silica surface. As seen in Fig. 2 and Table 1, the grafting procedure does not significantly modify the structural properties of the support. The d_{100} reflection in the X-ray powder diffraction pattern does not change upon grafting and subsequent calcination. The BET surface area and pore diameter are also similar before and after treatment, indicating that the macroscopic structure of calcined SBA-15 is thermally and chemically stable. This is not the case when SBA-15 is impregnated with titanium isopropoxide in ethanol [32]. It has been reported that the BET surface area decreased by more than 25% for a sample with Ti loading corresponding to Si/Ti = 40. At the same time, the pore diameter also decreased and this was attributed to the formation of a titanium oxide layer on the surface of the mesopores. Moreover, the maximum of the UV–visible absorption band was shifted to near 270 nm. This is not the case for our samples and will be discussed later.

Table 1
Structural and physico-chemical properties of the materials

Sample	Si/Ti	S (m^2/g)	V (cm^3/g)[a]	a_0 (Å)	Φ_p (Å)
SBA-15	∞	987	1.35	106	66
TiSBA-100	98	972	1.29	105	68
TiSBA-50	52	924	1.33	105	67
TiSBA-30	33	1004	1.32	106	67
TiHMS-100	109	1023	1.12	53	34
TiHMS-50	54	1124	1.05	52	35
TiHMS-30	29	987	0.87	50	32
TiHMS-10	11	788	0.56	46	28

[a] Volume measured at $p/p_0 = 0.85$ for TiSBA materials and $p/p_0 = 0.5$ for HMS compounds.

3.3. Characterization of TiHMS materials

The XRD pattern of calcined TiHMS-100 is composed of a major broad reflection around 2° along with a minor signal at ca. 4° (Fig. 4). This corresponds to a unit cell parameter $a_0 \approx 53$ Å. The fact that reflections are broad and not resolved results from the relatively short-range order of the structure as compared to highly ordered materials like SBA-15 or MCM-41. All TiHMS materials show a similar X-ray pattern but the unit cell parameter slightly decreases from 53 to 46 Å with the Ti content (Fig. 4). At the same time, the intensity of the major XRD reflection decreases, indicating that the incorporation of titanium modifies the structure of the solid. The Si/Ti ratios in calcined solids are very close to those of the synthesis gels (Table 1). All catalysts exhibit a type IV isotherm with a well-defined step around $p/p_0 = 0.4$ (Fig. 5). The step is less abrupt and shifted to a lower pressure value for sample TiHMS-10 with the highest Ti content, indicating that mesopores are less regular than in samples with lower Ti contents. All materials possess high BET surface areas between 788 and 1124 m^2/g. The surface area has a tendency to decrease with the Ti content, as already reported [21,25].

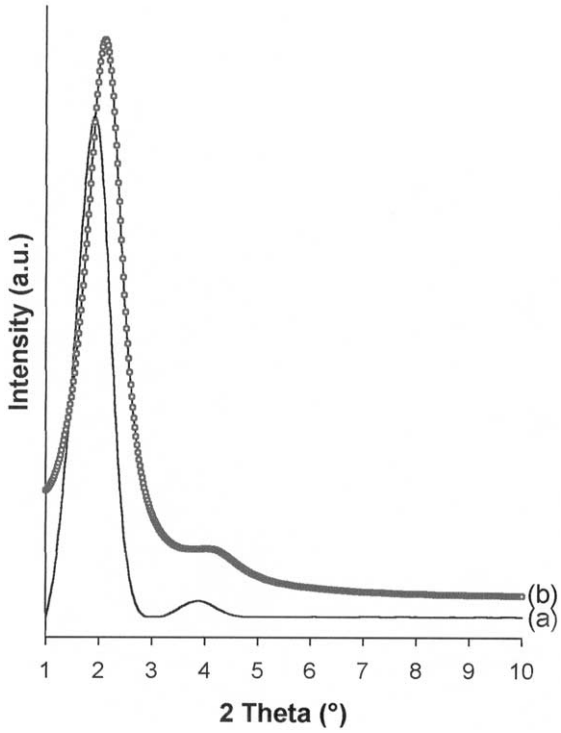

Fig. 4. X-ray diffraction patterns of calcined TiHMS-100 (a) and TiHMS-10 (b).

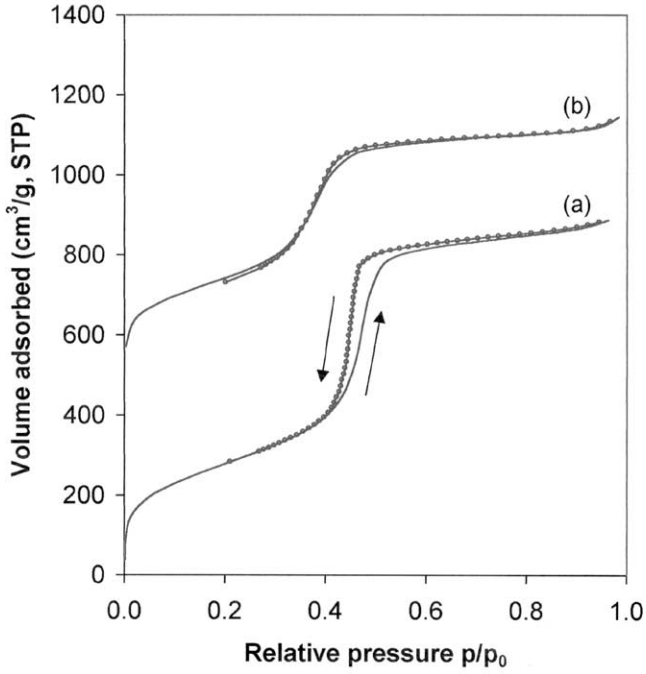

Fig. 5. Nitrogen adsorption/desorption isotherms on TiHMS-100 (a) and TiHMS-10 (b) materials.

3.4. UV–visible spectroscopy

UV–visible spectroscopy is commonly used to characterize the dispersion of titanium in Ti-containing inorganic materials. This technique is not quantitative: neither the exact coordination state nor the diameter of TiO_2 nanoparticles can be directly deduced from the spectra. Nevertheless, it is well established that charge transfers around 210–220 nm characterize isolated, tetrahedrally coordinated Ti species. The best example is TS-1 for which the UV absorption band is observed at ca. 210 nm on the dehydrated material [19]. On the other hand, UV–visible signals above 300 nm can be assigned to oxide nanoparticles. For TiO_2 particles, it has been reported that the absorption edge increases with dispersion from ca. 300 nm for nanoparticles up to 360–370 nm for bulk anatase [33]. However, spectra generally result from the superposition of signals due to a broad particle-size distribution, and direct measurement of the particle size from the absorption edge value is not possible. The assignment of UV–visible signals in the intermediate region, i.e., between 230 and 300 nm, is more controversial. Indeed, within this region, the maximum of absorption is not only sensitive to dispersion but also to the hydration state. Spectra are thus strongly dependent on the experimental conditions [33,34]. This is clearly illustrated by the spectra of our TiSBA materials (Fig. 6). Dry as-made materials show a unique absorption band with a maximum between 230 and 240 nm. The absence of significant absorptions above 300 nm is a good indication that large TiO_2 particles have not been formed during grafting. A shoulder, observed around 280 nm (spectrum TiSBA-100(AS)), can be assigned to solvent, water, or carbonaceous residues resulting from the hydrolysis of the cluster. This shoulder disappears upon calcination in air at high temperature. Thermal analysis followed by mass spectrometry performed on TiSBA-30 shows that the major weight loss occurs below 200 °C and corresponds to the removal of water and THF. A minor loss (<10%) is visible around 375 °C and results from the decomposition of organics. From the latter weight loss, we can estimate that less than 10% of the ligands of the clusters are present on silica after grafting.

The spectra of calcined TiSBA compounds are similar to those of the corresponding TiHMS materials (Fig. 6). They differ essentially in the region below 230 nm, where a relatively intense signal is observed for TiHMS but not for TiSBA compounds. This signal corresponds to Ti atoms with a 4-fold coordination. Therefore, UV–visible spectroscopy clearly indicates that a significant proportion of Ti sites in TiHMS materials probably possesses an octahedral coordination and appears as small subnanometric particles. The presence of such nanoparticles with absorptions below 250 nm is rarely noted in the literature. Signals around 230–240 nm are generally assigned to isolated Ti species with a 5- or 6-fold coordination. Some authors even report UV–visible spectra of TiMCM-41 materials with bands centered at 265 nm and assign them to a charge transfer between tetrahedral oxygen ligands and Ti^{4+} ions [35]. This assignment is controversial, the signals being rather characteristic of highly dispersed TiO_2 nanoparticles.

The maximum of absorption is slightly shifted with Ti loading from 233 nm for TiSBA-100 to 240 nm for TiSBA-30 (Fig. 6). This suggests the formation of larger particles

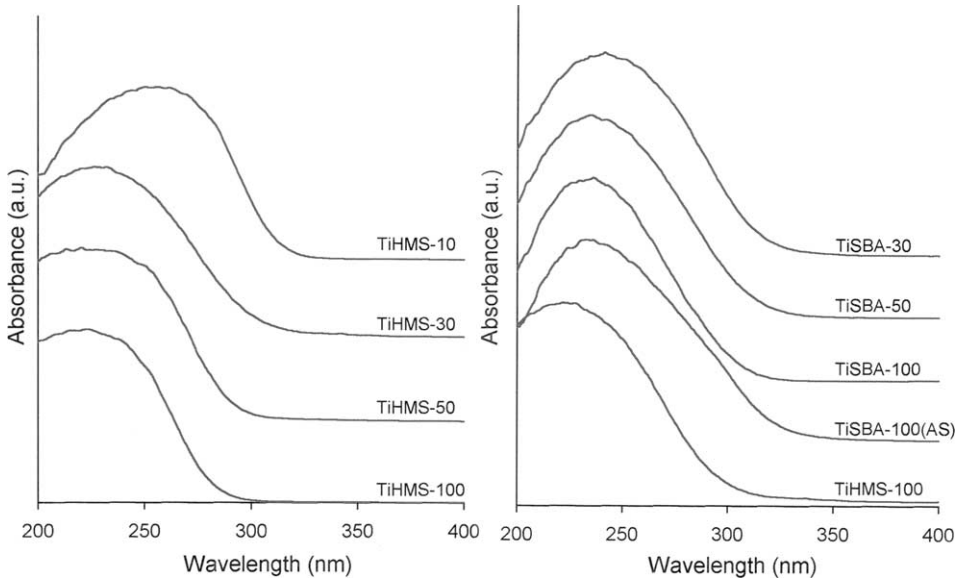

Fig. 6. Normalized UV–visible spectra of calcined TiHMS (left) and TiSBA (right) catalysts. TiHMS-100(AS) has been recorded on the as-made catalyst prior to calcination.

on the surface of TiSBA-30. These particles may be formed during grafting by condensation of two or more Ti_6 clusters. Nevertheless, the shift is limited to a few nanometers, which indicates that the proportion of clusters containing more than 6 Ti atoms is very low. This is not the case for TiHMS materials prepared with high Ti loading. For TiHMS-10, the maximum of absorption is located around 270 nm in the dehydrated form, which is consistent with a high amount of relatively large TiO_2 particles.

The maximum of the UV–visible absorption band strongly depends on the hydration state of the compounds. As seen in Fig. 7, the signal of TiSBA materials immediately changes upon hydration at room temperature. The maximum is shifted by about 15 nm and a broad band is observed between 350 and 500 nm. These changes are reversible and the original spectrum is restored upon evacuation at 200 °C. A similar behavior has been observed on Ti-substituted mesoporous silicas. It was attributed to a modification of the coordination state of Ti species [20,25]. In TiSBA materials, all Ti species are octahedrally coordinated, even in the dehydrated form. During the grafting procedure, the complete hydrolysis of Ti_6 clusters leads to the formation of 12 $Ti–O^-$ bonds per cluster. Some of them react with silanol groups of the silica surface to form Ti–O–Si bridges while others react with water molecules to form Ti–OH groups. The latter can further react like silanol groups and form hydrogen bonds with water molecules. The facile hydrolysis of Si–O–Ti bonds may also explain the reactivity of TiSBA compounds toward water.

The immediate modification of the spectrum indicates that all Ti species are very accessible to water molecules. This is a consequence of the location of Ti_6 cluster on the surface of the mesopores and this contrasts with TiHMS compounds where a significant proportion of Ti species is

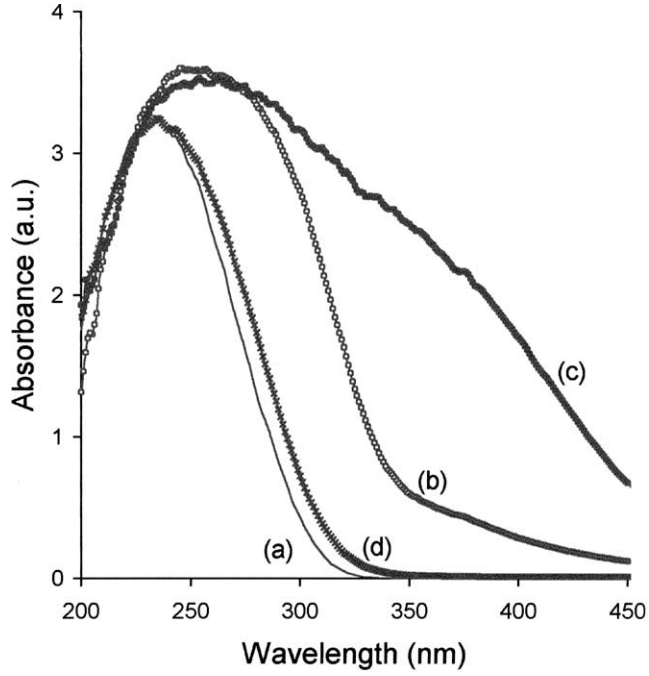

Fig. 7. Normalized UV–visible spectra of dry TiSBA-100 (a), after adsorption of water (b), and after adsorption of hydrogen peroxide (c). Spectrum (d) corresponds to TiSBA-100 recovered after 3 catalytic runs in the oxidation of aniline with H_2O_2 (see Table 3).

located inside the silica walls and are not easily accessible to water. The difference is even more pronounced upon dehydration. While TiSBA materials are completely dehydrated upon heating at 150 °C for 1 h, TiHMS materials still contain water after heating for 4 h at the same temperature.

Ti_6 clusters in TiSBA materials also react with hydrogen peroxide solutions. When a dry TiSBA compound is contacted with an aqueous H_2O_2 solution (30 wt%), the color immediately changes from white to bright yellow, indicating

the formation of titanium peroxo species [36,37]. The resulting material is characterized by a very broad UV–visible absorption around 350 nm (Fig. 7). Upon heating the solid at 60 °C for 1 h, the color turns back to white. The broad UV–visible signal disappears and the spectrum of the solid (not shown) is similar to that of the original dry TiSBA. As for water molecules, peroxo species probably result from the reaction between Ti–OH groups or Si–O–Ti bridges with H_2O_2.

3.5. Catalytic activity

3.5.1. Epoxidation of cyclohexene

SiO_2–TiO_2 mixed oxides are efficient catalysts in the epoxidation of olefins with alkyl hydroperoxides like TBHP. Preliminary experiments showed that the dispersion of Ti on silica was a critical parameter [1–3]. Further studies confirmed this observation and it was suggested that the active sites for the reaction were tetrahedrally coordinated Ti species [38,39]. However, excellent activities and selectivities to epoxides were reported for catalysts containing more than 30 mol% Ti [40,41]. Characterization of these catalysts by UV–visible spectroscopy, XANES, or EXAFS clearly showed that they did not contain only tetrahedrally coordinated titanium but also Ti species with 5- and 6-fold coordination [20,31,42–44]. This suggests that the coordination state of Ti species is not the only factor that affects the activity in epoxidation. Other parameters like the acidity of the support, the nature and accessibility of Ti species, and the particle size probably also influence the catalytic performance.

TiSBA materials are active in the epoxidation of cyclohexene with TBHP. The catalytic performances are reported in Table 2 and compared with those obtained on TiHMS compounds. With TBHP, the only product detected is cyclohexene oxide with a selectivity close to 100%. Whatever the Ti content, the TBHP conversion is always complete after 1 h when the reaction is performed over TiSBA. By contrast, only 76% of the oxidant is consumed over TiHMS-100 and the percentage increases with the Ti content. The superiority of TiSBA compounds over TiHMS in the catalytic epoxidation of cyclohexene is clearly shown in Table 2. For TiSBA materials, the initial rate, defined as the epoxide formation within the first 100 s, increases proportionally to the Ti content. Actually, the TBHP conversion is almost complete after 10 min on TiSBA-30. We observe the same evolution over TiHMS materials, at least for low Ti contents; however, the initial rate is low compared to that obtained on TiSBA materials. The higher activity of TiSBA catalysts probably results from a better accessibility of cyclohexene molecules to Ti sites. Differences in catalytic performance between mesoporous materials prepared by direct synthesis and postsynthesis grafting have already been reported by Oldroyd et al. [45]. These authors compared the catalytic activity of TiMCM-41 materials in the epoxidation of olefins by various alkyl hydroperoxides. The grafted catalyst was about 10 times more active than the catalyst prepared by direct synthesis.

Table 2
Cyclohexene epoxidation with TBHP over the various materials[a]

Catalyst	TBHP conv. (%)	Initial rate (mmol/(min g))	Selectivity (%)	
			S_{per}[b]	S_{epo}[c]
TiSBA-100	99	1.71	95	100
TiSBA-50	100	3.80	94	98
	99[d]	4.05	95	100
	100[d]	3.92	91	100
TiSBA-30	100	5.82	92	99
TiHMS-100	76	0.37	95	100
TiHMS-50	89	1.03	94	99
TiHMS-30	99	2.03	89	98
TiHMS-10	100	1.61	78	100

[a] Experimental conditions: 0.25 mol cyclohexene, 0.05 mol TBHP, 20 mL 2-methoxyethylether (solvent), 0.5 g catalyst. $T = 80\,°C$, reaction time: 3 h.

[b,c] The TBHP and epoxide selectivities are calculated as follows: S_{per} (%) $= 100 \times [\text{epoxide}]_f/([\text{peroxide}]_i - [\text{peroxide}]_f)$, S_{epo} (%) $= 100 \times [\text{epoxide}]_f/([\text{cyclohexene}]_i - [\text{cyclohexene}]_f)$, where i and f stand for initial and final concentration values, respectively.

[d] Catalyst recycling: the reaction was repeated three times with the same catalyst. Before the second and third reactions, the catalyst was recovered and washed with 25 mL 2-methoxyethylether.

Our results also indicate that Ti_6 clusters do not migrate into the micropores of SBA-15 during calcination. For TiHMS-10, the activity is relatively low and the catalyst is less active than TiHMS-30. As previously noted, this solid is less ordered than the others, with a lower surface area and smaller pore diameter. These structural parameters probably affect the catalytic performance by decreasing the diffusion of reactants and products inside the mesopores. Moreover, UV–visible spectroscopy indicated that Ti species were not highly dispersed in this catalyst. Larger TiO_2 particles are known to inhibit epoxidation reactions by decreasing the number of accessible catalytic sites and by favoring the peroxide decomposition [40,41].

The stability of TiSBA catalysts under reaction conditions has been studied over TiSBA-50 and results are listed in Table 2. Neither the initial activity nor the selectivities changed after three successive runs. Chemical analysis and UV–visible spectroscopy indicated that the Ti content and dispersion were unchanged, and that no Ti leaching had occurred.

3.5.2. Oxidation of aniline

We have previously reported that Ti-substituted mesoporous silicas are excellent catalysts in the oxidation of aniline and substituted anilines with hydrogen peroxide [11,46, 47]. The activity of the catalysts is far superior to that of zeolites like TS-1. Indeed, the size of reactants and products is such that diffusion greatly limits the reaction when microporous catalysts like TS-1 are used. At high temperature ($> 60\,°C$), the reaction is complex and proceeds via the formation of phenylhydroxylamine and nitrosobenzene. These two products further react together to form azoxy-

Table 3
Aniline oxidation over TiSBA and TiHMS materials[a]

Catalyst	Oxidant	Initial rate (mmol/(min g))	S_{per}[b]	Product selectivity (%)	
				AZY[c]	AZO[c]
TiSBA-100	H_2O_2	–	92	92	8
			94[d]	95	5
			93[d]	93	7
	TBHP	0.22	77	75	25
TiSBA-50	H_2O_2	–	97	95	5
	TBHP	0.41	75	77	23
TiSBA-30	H_2O_2	–	87	85	15
	TBHP	0.57	79	75	25
TiHMS-100	H_2O_2	–	89	88	12
	TBHP	0.09	83	78	22
TiHMS-50	H_2O_2	–	95	90	10
	TBHP	0.20	75	79	21
TiHMS-30	H_2O_2	–	97	94	6
	TBHP	0.31	79	75	25
TiHMS-10	H_2O_2	–	72	78	22
	TBHP	0.35	78	73	27

[a] Reaction conditions: 0.5 g catalyst, 4.6 ml aniline (5×10^{-2} mol), 20 mL acetonitrile (solvent), oxidant/aniline = 0.2, $T = 70\,^{\circ}C$, reaction time = 5 h.

[b] Peroxide selectivity defined as in Table 2.

[c] Azoxybenzene and azobenzene selectivities. AZY = [azoxybenzene]/Σ, AZO = [azoxybenzene]/Σ with Σ = [azoxybenzene] + [azobenzene].

[d] Catalyst recycling: the reaction was repeated 3 times with the same catalyst. Before the second and third reaction, the catalyst was recovered, washed with acetonitrile, and calcined in air at 500 °C.

benzene. Preliminary results indicated that TiHMS materials with Si/Ti ratios between 30 and 85 were very active in this reaction and that the initial rate of formation of azoxybenzene was proportional to the Ti content. High activities were also observed when the reaction was performed with TBHP as oxidizing agent.

TiSBA materials are active catalysts in the oxidation of aniline with hydrogen peroxide and TBHP (Table 3). With both oxidants, azoxybenzene is the major product formed, as expected at the temperature of the reaction. With H_2O_2, the reaction is extremely fast and more than 90% of the peroxide is consumed within the first 10 min. It was thus not possible to estimate the rate constant of formation of azoxybenzene for a given catalyst, but we could observe that it increased with Ti loading. Because of the rapidity of the reaction, a comparison of the performances of TiSBA and TiHMS catalysts was difficult. Table 3 shows that the azoxybenzene and H_2O_2 selectivities slightly decrease for TiSBA-30 and TiHMS-10. Moreover, the azobenzene selectivity increases, suggesting that TiO_2 particles with more than 6 Ti atoms may favor the decomposition of H_2O_2. Indeed, we have previously proposed that the formation of radicals by metal-catalyzed decomposition of hydrogen peroxide could lead to the direct formation of azobenzene [11].

The rate of formation of azoxybenzene is considerably lower when the reaction is performed with TBHP. The measurement of reaction rates and the comparison between TiSBA and TiHMS catalysts are thus possible. By contrast to reactions performed with H_2O_2, nitrosobenzene is not detected, even at the beginning of the reaction. Azobenzene is formed as a secondary product, probably by decomposition of the peroxide and formation of radicals. This assumption is supported by the slightly higher selectivity in azobenzene over Ti-rich catalysts, in particular TiHMS-10 in which Ti species are essentially in the form of large oxide particles.

For TiSBA catalysts, the initial rate of formation of azoxybenzene increases almost linearly with Ti loading, thus confirming that the reaction is not limited by diffusion. By contrast to experiments performed with H_2O_2, the azoxybenzene selectivity does not significantly decrease over TiSBA-30, suggesting that TBHP is less sensitive than H_2O_2 to the presence of large TiO_2 particles. TiHMS catalysts are also active in the oxidation of aniline with TBHP but activities are always lower than those of TiSBA materials. As for epoxidation reactions, this can be attributed to the existence of internal sites in HMS materials, not accessible to substrate and oxidant molecules.

Recycling experiments have been performed over TiSBA-100 to check the stability of the catalyst in the presence of hydrogen peroxide. After each reaction, the catalyst was recovered by filtration, washed with acetonitrile, and calcined in air at 500 °C. Catalytic data indicate that the peroxide selectivity remains very high and that the product distribution is not significantly affected after 3 runs. Fig. 7d, shows the UV–visible spectrum of TiSBA-100 recovered after the third run and subsequently washed and calcined. Clearly, the maximum of absorption is unchanged compared to the fresh catalyst, and this demonstrates that hydrogen peroxide does not modify the dispersion of TiO_2 particles on the silica surface under reaction conditions.

3.5.3. Oxidation of aromatic compounds

2,6-Di-*tert*-butylphenol is one of the large substrates that cannot be oxidized over microporous zeolites but relatively easily over Ti-substituted mesoporous silicas. Pinnavaia et al. first reported that TiHMS materials convert DTBP into the corresponding quinone using dilute solutions of hydrogen peroxide [12]. The conversion was generally low, a significant proportion of H_2O_2 being decomposed under reaction conditions. High conversions could only be obtained using a large excess of H_2O_2 with respect to the substrate. For a H_2O_2:substrate ratio of 6:1, the DTBP conversion increased with Ti loading, from 26% for a catalyst containing 1 mol% Ti to 98% for a catalyst with 10 mol% Ti. The catalyst with 10 mol% Ti probably contained polycondensed Ti species, as is the case for our TiHMS-10 material. Thus, experimental data suggest that the reaction is not very sensitive to the dispersion of Ti species and that good activities can be obtained over TiO_2 nanoparticles.

This is what we observe experimentally on the series of TiSBA catalysts (Table 4). For a H_2O_2:substrate ratio of 6:1, the DTBP conversion increases from 30 to 77% with Ti loading. Experiments performed under the same conditions on TiHMS materials with similar Ti loading give conversions from 25 to 74%. With TiHMS-10, 89% of the substrate is

Table 4
Oxidation of 2,6-di-*tert*-butylphenol over TiSBA and TiHMS catalysts[a]

Catalyst	DTBP Conv. (%)	H_2O_2 Selectivity (%)	Quinone[b] (%)
TiSBA-100	30	25	100
TiSBA-50	57	33	98
TiSBA-30	77	31	98
TiHMS-100	25	11	98
TiHMS-50	60	15	99
TiHMS-30	74	22	100
TiHMS-10	89	32	91

[a] Reaction conditions: 0.5 g catalyst; H_2O_2/DTBP = 6; solvent, acetone; $T = 70\,^{\circ}C$; reaction time, 3 h.
[b] Other products are essentially the binuclear di-*tert*-butylquinone.

converted after 2 h, a value quite similar to that reported by Pinnavaia et al. [12] on the same type of materials. The similarity between DTBP conversions obtained on TiSBA and TiHMS catalysts is evidence that active species are not necessarily 4-coordinated Ti species.

Similar conclusions can be drawn from the oxidation 2,3,6-trimethylphenol. This oxidation is of practical importance for the production of 2,3,6-trimethylbenzoquinone (TMBQ), an intermediate in the synthesis of vitamin E. Catalytic routes based mainly on the use of homogeneous catalysts have been developed to produce TMBQ from TMP. However, Sorokin and Tuel showed that excellent TMP conversions and TMBQ yields could be obtained over TiMCM-41 catalysts using both H_2O_2 and TBHP as oxidants [48]. Trukhan et al. [21] investigated the influence of Ti loading and structure regularity on the catalytic performance of Ti-containing mesoporous materials. They observed that both the TMP conversion and the TMBQ selectivity first increased with Ti loading up to ca. 2 wt% Ti and then decreased monotonously. They concluded that a high dispersion of Ti species is a necessary condition for a good catalytic activity in this reaction. However, by comparing a highly ordered TiMCM-41 with a less regular TiHMS catalyst, they found that the regularity of the structure also influences the catalytic results.

As seen in Table 5, TiSBA materials catalyze the oxidation of TMP with hydrogen peroxide. Conversions and TMBQ selectivities are comparable and sometimes higher than those obtained over TiHMS materials having the same Ti loading. Thus, the absence of isolated Ti sites with a 4-fold coordination does not seem to be detrimental to the catalytic activity. Actually, the decrease in activity reported for Ti-substituted MCM-41 with high Ti loading most likely results from a loss of Ti accessibility. Indeed, many papers report that the intensity of the d_{100} as well as the resolution of d_{110} and d_{200} reflections in the XRD patterns of TiMCM-41 materials decrease with Ti loading, suggesting a loss of long-range ordering. Moreover, the silica wall thickness generally increases with Ti loading. Therefore, the fraction of Ti sites located inside the walls also increases whereas that of surface sites, effectively accessible to substrate molecules and active in the catalytic reaction, decreases.

Table 5
Oxidation of 2,3,6-trimethylphenol over TiSBA and TiHMS catalysts[a]

Catalyst	TMP Conv. (%)	H_2O_2 Selectivity (%)[b]	TMQ Selectivity (%)
TiSBA-100	98	46	95
TiSBA-50	97	46	96
TiSBA-30	99	48	97
TiHMS-100	92	44	97
TiHMS-50	97	48	98
TiHMS-30	99	47	95
TiHMS-10	99	46	93

[a] Reaction conditions: 0.5 g catalyst; 13.6 g (0.1 mol) TMP; 20 mL acetonitrile (solvent); H_2O_2/TMP = 4; $T = 80\,^{\circ}C$; reaction time, 3 h. H_2O_2 was added by portions at $t = 0$, 30 min, 1, and 1.5 h. Reactions were run for 1.5 h after the complete addition of H_2O_2.
[b] For all reactions, H_2O_2 was completely consumed after 3 h.

Many authors have reported that the oxidation of phenol derivatives proceeds via the formation of phenoxyl radicals [49]. Initially, radicals are produced by the decomposition of peroxo titanium species formed by reaction between H_2O_2 and titanium sites

$$\text{Ti–OH} + H_2O_2 \rightarrow \text{TiOOH} + H_2O, \quad (1)$$

$$\text{TiOOH} \rightarrow \text{TiO}^{\bullet} + {}^{\bullet}\text{OH}, \quad (2)$$

$$\text{TiO}^{\bullet} + H_2O \rightarrow \text{TiOH} + {}^{\bullet}\text{OH}. \quad (3)$$

These radicals further react with aromatic molecules to form phenoxyl radicals,

$$\text{ArOH} + {}^{\bullet}\text{OH} \rightarrow \text{ArO}^{\bullet} + H_2O \rightarrow \text{quinone}, \quad (4)$$

or form oxygen and water by self-reaction,

$$2\,{}^{\bullet}\text{OH} \rightarrow H_2O + \tfrac{1}{2}O_2. \quad (5)$$

The rate of decomposition of hydrogen peroxide depends essentially on the dispersion and accessibility of titanium sites. By contrast to large TiO_2 domains, highly dispersed particles will favor the decomposition of H_2O_2. This could explain the poor activity of catalysts containing more than 10 mol% Ti, in which large TiO_2 particles are certainly present. The formation of quinones [Eq. (4)] is in competition with that of oxygen [Eq. (5)]. The last reaction occurs on TiSBA as well as TiHMS catalysts and is responsible for the relatively high H_2O_2 decomposition.

4. Concluding remarks

A hexanuclear titanium cluster has been grafted on a mesoporous silica SBA-15. The material thus obtained has been used as a "model compound" for testing the catalytic properties of monodispersed subnanometric TiO_2 particles in oxidation reactions in the liquid phase. UV–visible spectroscopy shows that the grafted silica is characterized by an absorption band at ca. 235 nm. This value is not very different from that observed on Ti-modified catalysts obtained by direct synthesis. This suggests that large TiO_2 domains

have not been formed upon grafting and that Ti_6 clusters are well dispersed on the surface of silica. Unfortunately it is not possible to obtain the real size of Ti aggregates from UV–visible spectra. The titanium particle in the initial Ti_6 cluster possesses a size of ca. 8 Å. It is reasonable to assume that the size is not very different after grafting on silica. Further treatments like calcination may induce a modification of the size of the clusters by changing the assembly of Ti atoms. However, the maximum of the UV–visible absorption band does not change upon calcination, and this strongly suggests that the size of TiO_2 particles remains practically unchanged, i.e., below 1 nm.

Catalytic experiments clearly show that such TiO_2 nanoparticles are active and selective in oxidation reactions using H_2O_2. Many authors have reported that the active sites in oxidation reactions are Ti atoms with 4-fold coordination and that the presence of polycondensed species reduces the activity. However, the coordination of Ti species is often estimated from the position of UV–visible absorption bands. We have seen that these bands cannot be unambiguously assigned to a specific coordination state, in particular when the maximum of absorption is between 230 and 250 nm. Whereas some authors consider that polycondensed Ti species are already present in catalysts with an absorption band at 230 nm, UV–visible signals at 250 nm are sometimes assigned to a charge transfer between tetrahedral oxygen atoms and Ti^{4+} ions. This suggests that a majority of catalysts almost certainly contain TiO_2 nanodomains along with tetrahedrally coordinated Ti atoms. These nanodomains do not significantly decrease the catalytic performance of the solids. Hutter et al. previously suggested that well-dispersed small titania domains could be as active and selective as isolated Ti–O–Si species in epoxidation reactions. Indeed, they observed that the activity of TiO_2–SiO_2 mixed oxides in the epoxidation of cyclohexene with cumene hydroperoxide increased with Ti loading up to 20 wt%. At the same time, the size of TiO_2 domains also increased, as evidenced by the shift of the UV–visible absorption edge from ca. 280 to 340 nm.

All these observations tend to confirm that, for Ti-containing catalysts, a high activity does not necessarily mean that catalysts are free from TiO_2 particles and contain only tetrahedrally coordinated species. They also suggest that the decrease in activity usually observed at high Ti loading must not be systematically attributed to polycondensed species with 6-fold coordination. Other parameters like the accessibility to active sites, the presence of large TiO_2 particles, and the extent of peroxide decomposition must also be considered.

Acknowledgment

The authors thank Y. Lakhdar for providing the hexanuclear titanium cluster.

References

[1] UK patent 1,249,079, 1971.
[2] US patent, 3,923,843, 1975.
[3] R.A. Sheldon, J. Mol. Catal. 7 (1980) 107.
[4] US patent 4,410,501, 1983.
[5] B. Notari, Catal. Today 18 (1993) 163.
[6] U. Romano, A. Esposito, F. Maspero, C. Neri, M.G. Clerici, Chim. Indust. 72 (1990) 610.
[7] A. Corma, M.T. Navarro, J. Perez-Pariente, J. Chem. Soc., Chem. Commun. (1994) 147.
[8] P.T. Tanev, M. Chibwe, T.J. Pinnavaia, Nature 368 (1994) 321.
[9] O. Franke, J. Rathousky, G. Schulz-Ekloff, J. Starek, A. Zukal, Stud. Surf. Sci. Catal. 84 (1994) 77.
[10] T. Blasco, A. Corma, M.T. Navarro, J. Perez-Pariente, J. Catal. 156 (1995) 65.
[11] S. Gontier, A. Tuel, J. Catal. 157 (1995) 124.
[12] T.J. Pinnavaia, P.T. Tanev, J. Wang, W. Zhang, in: Sh. Komarneni, J.S. Beck, D.M. Smith (Eds.), Advances in Porous Materials, in: MRS Symposium Proceedings Series, MRS, Pittsburgh, PA, 1995, p. 53.
[13] A. Tuel, Micropor. Mesopor. Mater. 27 (1999) 151.
[14] A. Tuel, Stud. Surf. Sci. Catal. 117 (1998) 159.
[15] A. Sayari, Chem. Mater. 8 (1996) 1840.
[16] A. Tuel, J. Diab, P. Gelin, M. Dufaux, J.F. Dutel, Y. Ben Taarit, J. Mol. Catal. 63 (1990) 95.
[17] G. Deo, A.M. Turek, I.E. Wachs, D.R.C. Huybrechts, P.A. Jacobs, Zeolites 13 (1993) 365.
[18] D.R.C. Huybrechts, P.L. Buskens, P.A. Jacobs, J. Mol. Catal. 71 (1992) 129.
[19] A. Zecchina, G. Spoto, S. Bordiga, A. Ferrero, G. Petrini, G. Leofanti, M. Padovan, Stud. Surf. Sci. Catal. 69 (1991) 251.
[20] W. Zhang, M. Fröba, J. Wang, P.T. Tanev, J. Wong, T.J. Pinnavaia, J. Am. Chem. Soc. 118 (1996) 9164.
[21] N.N. Trukhan, V.N. Romannikov, E.A. Paukshtis, A.N. Shmakov, O.A. Kholdeeva, J. Catal. 202 (2001) 110.
[22] M. Iwamoto, Y. Tanaka, J. Hirosumi, N. Kita, S. Triwahyono, Micropor. Mesopor. Mater. 48 (2001) 217.
[23] R. Papiernik, L.G. Hubert-Pfalzgraf, J. Vaissermann, M.C. Henriques Baptista Goncalves, J. Chem. Soc., Dalton Trans. 14 (1998) 2285.
[24] D. Zhao, J. Sun, Q. Li, G.D. Stucky, Chem. Mater. 12 (2000) 275.
[25] S. Gontier, A. Tuel, Zeolites 15 (1995) 601.
[26] L.G. Hubert-Pfalzgraf, New J. Chem. 11 (1987) 663.
[27] L.G. Hubert-Pfalzgraf, Appl. Organometal. Chem. 6 (1992) 627.
[28] C. Sanchez, J. Livage, New J. Chem. 14 (1990) 513.
[29] D. Zhao, J. Feng, Q. Huo, N. Melosh, G.H. Fredrickson, B.F. Chmelka, G.D. Stucky, Science 279 (1998) 548.
[30] D. Zhao, Q. Huo, J. Feng, B.F. Chmelka, G.D. Stucky, J. Am. Chem. Soc. 120 (1998) 6024.
[31] M. Imperor, A. Davidson, Stud. Surf. Sci. Catal. 135 (2001), 08-O-03 (CD-ROM).
[32] Z. Luan, E.M. Maes, P.A.W. Van der Heide, D. Zhao, R.S. Czernuszewicz, L. Kevan, Chem. Mater. 11 (1999) 3680.
[33] S. Klein, B.M. Veckhuysen, J.A. Martens, W.F. Maier, P.A. Jacobs, J. Catal. 163 (1996) 489.
[34] X. Gao, S.R. Bare, J.L.G. Fierro, M.A. Banares, I.E. Wachs, J. Phys. Chem. B 102 (1998) 5653.
[35] Z. Luan, L. Kevan, J. Phys. Chem. B 101 (1997) 2020.
[36] D.R.C. Huybrechts, I. Vaesen, H.X. Li, P.A. Jacobs, Catal. Lett. 8 (1991) 237.
[37] F. Geobaldo, S. Bordiga, A. Zecchina, E. Giamello, G. Leofanti, G. Petrini, Catal. Lett. 16 (1992) 109.
[38] Z. Liu, G.M. Crumbaugh, R.G. Davis, J. Catal. 159 (1996) 83.
[39] S. Imamura, T. Nakai, H. Kanai, T. Ito, J. Chem. Soc., Faraday Trans. 91 (1995) 1261.
[40] D.C.M. Dutoit, M. Schneider, A. Baiker, J. Catal. 153 (1995) 165.
[41] R. Hutter, T. Mallat, A. Baiker, J. Catal. 153 (1995) 177.
[42] E. Jorda, A. Tuel, R. Teissier, J. Kervennal, J. Catal. 175 (1998) 93.
[43] Z. Liu, R.J. Davis, J. Phys. Chem. 98 (1994) 1253.

[44] S. Imamura, T. Nakai, H. Kanai, T. Ito, Catal. Lett. 28 (1994) 277.
[45] R.D. Oldroyd, J.M. Thomas, T. Maschmeyer, P.A. MacFaul, D.W. Snelgrove, K.U. Ingold, D.D.M. Wayner, Angew. Chem. Int. Ed. Engl. 35 (1996) 2787.
[46] S. Gontier, A. Tuel, Appl. Catal. 143 (1996) 125.
[47] S. Gontier, A. Tuel, Stud. Surf. Sci. Catal. 94 (1995) 689.
[48] A. Sorokin, A. Tuel, Catal. Today 57 (2000) 45.
[49] W.I. Taylor, Oxidative Couplings of Phenols, Dekker, New York, 1967.